Preparation of ZnWO₄ Nanopowders and Its Bulk Type Single Crystal Growth by the Czochralski Method†

C.S. LIM

Department of Advanced Materials Science and Engineering, Hanseo University, Seosan 356-706, South Korea

*Corresponding author: Tel/Fax: +82 41 6601445; E-mail: cslim@hanseo.ac.kr

ZnWO₄ nanopowders were prepared from polymeric complex method using microwave irradiation. The average crystalline sizes of the nanopowders were 18-25 nm showing an ordinary tendency to increase with the temperatures from 400 to 600 ºC. Bulk type single crystals of ZnWO₄ were grown successfully in the [100], [010] and [001] directions using the Czochralski method. The effect of the growth parameters, such as the rotation speed, pulling rate and diameter of the grown crystals, were examined. The dislocation density on the (010) plane at the center of the crystal was lower than near the edge. The etch pit arrangement revealed the (100) slip plane to be most active during crystal growth. The hardness, thermal expansion coefficients and dielectric constants of the crystals were evaluated.

Key Words: ZnWO₄, Nanopowders, Crystal growth, Czochralski method, Microstructure.

INTRODUCTION

ZnWO₄ is a technologically important material with a monoclinic wolframite-type structure in the space group P2/c. There are two formula units per primitive cell with lattice parameters of a = 4.69263 Å, b = 5.72129 Å, c = 4.92805 Å and β = 90.6321°[1]. In recent years, ZnWO₄ has attracted considerable attention for potential applications as a scintillator, maser, luminescent material and photocatalyst[2-7]. The physical, chemical and photochemical properties of ZnWO₄ are dependent on the manufacturing method. To enhance the applications of ZnWO₄, several processes have been developed over the last decade and can be classified. Usually, bulk type single crystal ZnWO₄ has been grown by the Czochralski method[7-10], whereas the powder form of ZnWO₄ has been prepared by different routes with a high quality for the application. ZnWO₄ nanoparticles have thus far been prepared by several different processes such as a solid-state reaction method[11], a co-precipitation method[12], from a molten salt[13], by combustion[14], a mechano-chemical method[15], a sol-gel method[16] and from a hydrothermal reaction[17-19].

To obtain pure powders, the conventional solid-state reaction methods have several problems, because the WO₃ has a tendency to vapourize at high temperatures, non-homogeneous compounds might be easily formed during the solid-state reaction processing and the temperature for the solid state

reaction is relatively high, almost above 1000 ºC for 24 h[20]. These problems could be solved by applying advanced wet chemical solution methods[21,22]. Polymerized complex method as a modified Pechini method[23], where several metal ions in a solution could be first chelated to form metal complexes and then polymerized to form a gel, seems to be most suitable among several chemical solution processes, because rigidly fixed cations are homogeneously dispersed in the polymer network and have few chances to segregate even during pyrolysis. This method has already successfully prepared highly pure samples of various double oxides such as BaTiO₃[24], Y₆WO₁₂[25], mixed-cation oxides[26] and even for various superconductors[27] with multiple cationic compositions.

However, in spite of the many advantages of the polymeric complex method, the weakness of the polymerized complex method is the difficulty of the effective removal of large amounts of organic substance. Based on this consideration, the citric acid complex as another chemical solution process was tried for the synthesis of ZnWO₄ nanopowders. There are several parameters for controlling the citric acid complex process to prepare ZnWO₄ particle with significant properties. Besides these established synthesis processes, finding simple and cost effective routes to synthesize ZnWO₄ is needed. Microwave irradiation as a heating method has found and developed a number of applications in chemistry and ceramic processing[28-31]. Compared with the usual method, microwave

†Presented to the 4th Korea-China International Conference on Multi-Functional Materials and Application.

synthesis has the advantages of very short reaction time, small particle size, narrow particle size distribution and high purity method in preparing nanocrystalline samples. Bi *et al.*[32] suggested that these advantages could be attributed to fast homogeneous nucleation and easy dissolution of the gel.

For high quality applications, $ZnWO_4$ single crystals are generally grown by the Czochralski method[7-10]. However, the problems associated with the crystal growth mechanisms and the crystal quality of $ZnWO_4$ are phenomenological in nature because of the complicated growth parameters of the interface between the solid and liquid. Stability with the growth parameters of $ZnWO_4$ single crystals are still a challenge for commercial applications. Therefore, for improved applications, a more detailed study of the growth mechanisms and characteristics of $ZnWO_4$ single crystals by the Czochralski method are needed.

In this study, the pure $ZnWO_4$ nanopowders were prepared from polymeric complex precursor using microwave. The $ZnWO_4$ nanopowders were evaluated in terms of the crystallization process, thermal decomposition and morphology. Bulk type single crystals of $ZnWO_4$ in the [100], [010] and [001] directions were grown successfully by the Czochralski method. The growth conditions in the [100], [010] and [001] directions were examined in terms of the rotation speed, pulling rate and diameter of the grown crystals. Subsequently, the physical properties of the grown crystals were evaluated in terms of hardness, thermal expansion coefficient and dielectric constants.

EXPERIMENTAL

Zinc acetate dihydrate [$Zn(CH_3COO)\cdot2H_2O$], Junsei Chemical Co. Ltd., Japan), tungstic acid (H_2WO_4, Acros Organics, USA), were used as metallic cations. De-ionized water (DW) and citric acid ($HOC(CO_2H)(CH_2CO_2H)_2$, CA, Yukiri Pure Chemical Co, Ltd., Japan) were used as polymerization/complex cation agents for the process. The citrate solution was prepared by dissolving appropriate molar ratios of citric acid in de-ionized water (CA:DW molar ratio = 1:4). After complete homogenization of the citrate solution, zinc acetate dehydrate and tungsten acid were dissolved in the molar ratio of total chelate metal cations (TO) and citric acid (TO:CA molar ratio = 1:5). By keeping the solution at a temperature of 50 ºC for 1 h under constant stirring, the solution became more viscous pale-yellow solution.

A domestic microwave oven with 650 W power (Samsung Electronic Corp. Korea) was conducted for the polymerizations of the precursors. The solution was placed in the microwave oven and the reaction was performed under ambient air for 0.5 h. The working cycle of the microwave oven was set between 30 s on and 30 s off. The solution became more viscous and changed its colour from pale-yellow to brown. Finally, the viscous solution was dried and a solidified dark brown glassy resin was formed. The resin was converted into powders after grinding with a Teflon bar. Thermal analysis was performed on this powder, hereinafter referred to as the 'precursor'. Heat-treatment of the precursor was performed at various temperatures from 300 to 600 ºC for 3 h.

The growth equipment for the Czochralski method was fabricated using a furnace assembly. The $ZnWO_4$ melts were prepared from polycrystalline $ZnWO_4$, placed in a platinum crucible. The platinum crucible was heated in a furnace fabricated with SiC resistive heating elements and the temperature was monitored and regulated using a controller and thyrister from Eurotherm Co. The single crystals were pulled along the crystallographic axes with a diameter of 0-3.5 cm at a pulling rate of 0-100 mm/h and a rotation speed of 0-68 rpm. The temperatures were controlled precisely with the measurements on the surface of the $ZnWO_4$ melts between 1230-1235 ºC during growth. The polycrystalline $ZnWO_4$ was prepared from stoichiometric amounts of the mole ratio of 1:1 for zinc oxide and tungsten trioxide. The mixed powders was pressed and calcined at 800, 900, 1000 and 1100 ºC for various times.

The phase in the powders after calcination was identified by X-ray diffraction (XRD, CuK$_\alpha$, 40 kV, 30 mA, Rigaku, Japan) at a scan rate of 3 ºC/min. Fourier transform infrared spectroscopy (FT-IR, Model IR 550, Magna, Nicolet Company) was used for the interpretation of the thermal-decomposition behaviour of the precursors and heat-treated powders in frequency ranges from 4000 to 400 cm^{-1}. The FT-IR spectra were measured in KBr pellets. The average crystallite size of the heat-treated powders was calculated using the XRD line broadening method through the Scherrer's relationship. The microstructure and surface morphology of the nanopowders were observed by scanning electron microscopy (SEM, JSM-35CF, JEOL) and transmission electron microscopy (TEM, JEM 2010, JEOL).

The microstructure of the etch pits were observed by optical microscopy and SEM. The dislocations in the cleaved slices were examined by chemical etching. The etched surfaces were obtained from a boiling 2 M NaOH solution. The (010) surface was etched in a boiling solution for 4 min, whereas the (001) and (100) surfaces were etched for 2 min. The hardness, thermal expansion coefficients and dielectric constants of the grown crystals were evaluated.

RESULTS AND DISCUSSION

Fig. 1 shows XRD results for the phase identification of the powders heated for 3 h as a function of heating temperature. In Fig. 1(a), the powders at 300 ºC were amorphous without any crystallized phases. Above 400 ºC, in Fig. 1(b-d) the peaks at 2θ = 23.8, 24.6, 30.5, 30.7, 31.3, 36.3 were $ZnWO_4$ (011), (110), (111), (111), (020), (021), respectively. All peaks in Fig. 1(b-d) are on basis of the crystallographic data of the
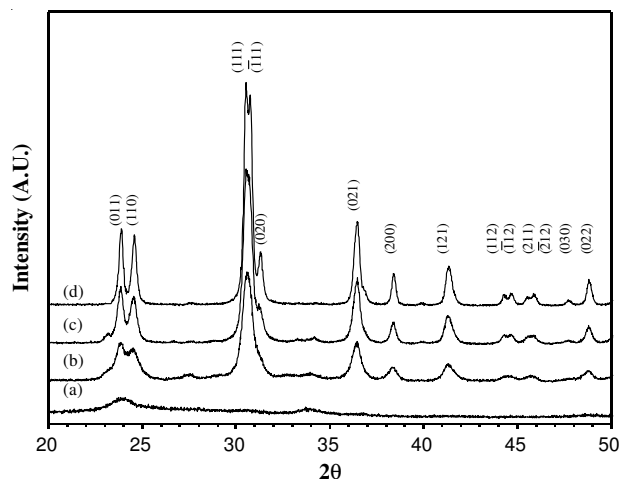

Fig. 1. XRD patterns of the $ZnWO_4$ nanopowders heat-treated at (a) 300, (b) 400, (c) 500 and (d) 600 ºC for 3 h

known structure of ZnWO$_4$ (JCPDS Code 15-0774), suggesting the lattice constants[1] are a = 4.69263 Å, b = 5.72129 Å, c = 4.92805 Å and β = 90.6321°.

Fig. 2(a-e) shows the FT-IR spectra for the precursor and powders heated at 300-600 °C. For the precursor (Fig. 2(a), the bands at 1620, 3445 cm^{-1} (O-H stretching modes), 1736, 1395 cm^{-1} (carboxyl group stretching modes), 1278 cm^{-1} (CH$_3$) and absorption bands near 877 cm^{-1} (W-O-Zn stretching mode) seem to define the relatively dehydrated (Zn·W)-citrate polymeric complex. Heat-treatment at 300 °C in Fig. 2(b) leads to a significant change in its infrared spectra. A decrease of the band at 1736, 1395 and 1620 cm^{-1} is produced, while the bands at 1278 cm^{-1} disappear. At 400 °C in Fig. 2(c), the bands of the carbonyl group disappear, while new absorption bands appear between 400 and 900 cm^{-1}. In Fig. 2(c-e), the bending and stretching vibrations of Zn-O (473, 532 cm^{-1}), W-O (633, 710 cm^{-1}) and Zn-O-W bond (834, 877 cm^{-1}) could be identified to the synthesized ZnWO$_4$.
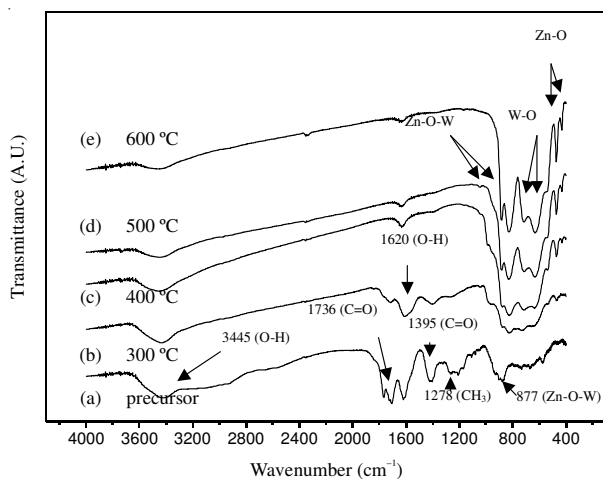

Fig. 2. FT-IR spectra of the ZnWO$_4$ (a) precursor and nanopowders heat-treated at (b) 300, (c) 400, (d) 500 and (e) 600 °C for 3 h

Fig. 3 shows TEM images of the ZnWO$_4$ nanopowders heat-treated at (a) 300, (b) 400, (c) 500 and (d) 600 °C for 3 h. The powders at 400 and 500 °C in Fig. 3(a) and (b) show primarily co-mixed morphology with spherical and silkworm-like forms. The particles at 500 °C in Fig. 3(c) have relatively more homogeneous morphology. The nanopowders at 600 °C in Fig. 3(d) show relatively exaggerated growth including rectangular powders. Table 1 shows the average crystallite sizes for the heat-treated nanopowders calculated by XRD line broadening method. The average crystallite size of the heat-treated nanopowders was calculated using the X-ray diffractometry line broadening method through the following Scherrer's equation[33].

$$D = K\lambda/(\beta\cos\theta) \qquad (1)$$

where D is the crystallite size, λ is wavelength of the radiation (λ = 1.5418 Å), θ is the Bragg's angle, β is the full width at half maximum (radian) and K is constant (0.9). The calculated average crystallite sizes in Table-1 were 18, 20, 23 and 25 nm for the heat-treated n nanopowders at 300, 400, 500 and 600 °C, respectively. These are corresponding to the TEM observations in Fig. 3 showing an ordinary tendency to increase with the temperatures from 400 to 600 °C.
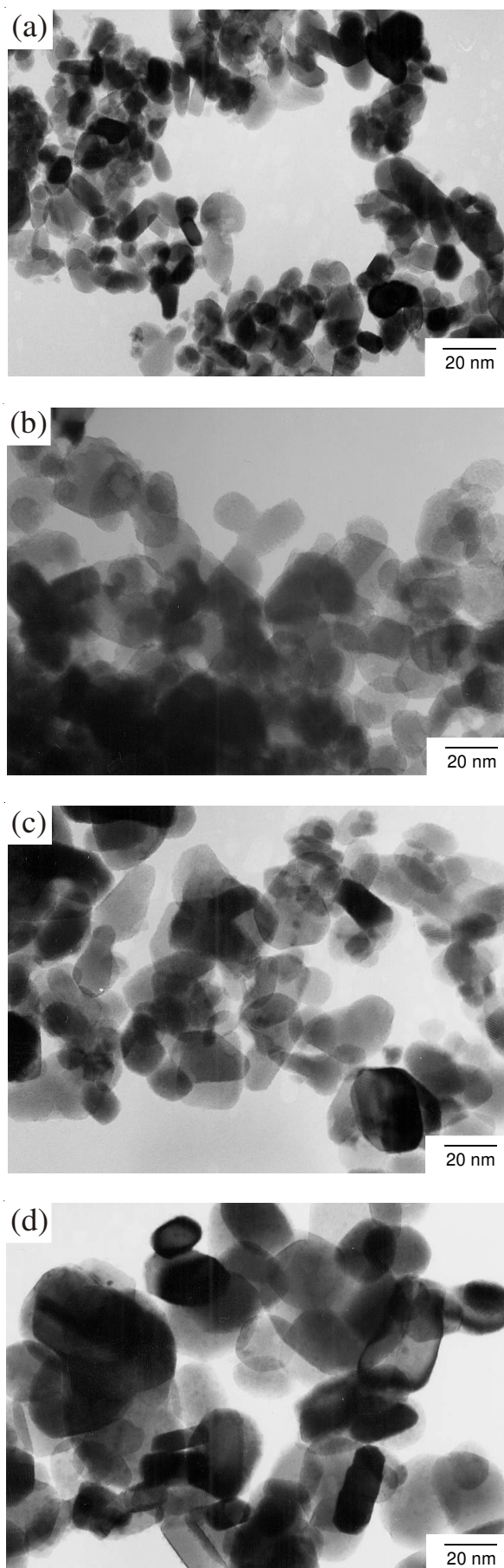

Fig. 3. TEM images of ZnWO$_4$ nanopowders heat-treated at (a) 300, (b) 400, (c) 500 and (d) 600 °C for 3 h

TABLE-1
AVERAGE CRYSTALLITE SIZE OF ZnWO₄ NANOPOWDERS AS A FUNCTION OF HEATING TEMPERATURE

Temperature (°C)	Average crystallite size (nm)
300	18
400	20
500	23
600	25

TABLE-2
TYPICAL GROWTH PROCEDURE AND PARAMETERS OF THE ZnWO₄ SINGLE CRYSTALS GROWN

Parameter procedure	Temperature (°C)	Pulling rate (mm/h)	Rotation speed (rpm)
Melting	1235	0.0	60
Dipping	1233	5.0	60
Necking	1234	8.0	60
Crowning	1231	3.5	60
Growing	1230	8-10	60
Tailing	1233	10	60

For the Czochralski growth of single crystals with a specific orientation, a seed crystal fixed properly to the pulling rod must be used. Platinum wires were used to obtain seed crystals employing capillary action from the melt. The platinum wires were dipped into the melt and the temperature was adjusted, a small crystal as a nucleus was grown inside the hole of the four platinum wires by capillary action. The temperature of the hole of the platinum wires was lower than the surface of the melt, so that nucleation occurred at a lower temperature. This crystal consisted of two crystals, due to heteronucleation during the dipping procedure at a lower temperature. The rotation speed was fixed to 40 rpm and the pulling rate was 0-10 mm/h. The maximum diameter was 1.9 mm and the crystal had a red-brown colour.

Seed crystals were fabricated with a length and diameter of 2.5 cm and 0.2 cm, respectively and employed for crystal growth along a crystallographic direction after identifying the crystal orientation by Laue back reflection. The ZnWO₄ single crystals were grown using the typical growth procedure and parameters listed in Table-2. The temperature was controlled between 1230-1235 °C, the rotation speed was fixed to 60 rpm and the pulling rate was between 0-10 mm/h. The grown crystals showed perfect cleavage on the (010) plane and the thin sections were found to cleave along the (101) plane. The (100) twin appeared to be the most common along the (101) plane.

For Czochralski growth, the crystal rotation speed and diameter were associated with the fluid-flow convection modes in the melt. Table-3 shows the crystal shape, rotation speed

and maximum diameter of the grown single crystals of ZnWO₄ grown. An increase in the crystal diameter results in an increase in the centrifugal force at the crystal periphery, which may bring a change in the fluid-flow convection of the liquid in contact with the growing interface. Table-3 shows the various crystal shapes according to rotation speeds of 15-68 rpm and a maximum diameter of 17-23 mm at a pulling rate of 0-10 mm/h.

Fig. 4 shows schematic diagrams of the relationships between the fluid-flowing convection models and interfacial shape at different crystal rotation speeds. Since the interfacial shape coincides with a freezing isotherm, this characteristic feature shows that the appearance of a concave interface is caused by fluid-flow rising from the central hot part of the melt, which is produced by an increase in the crystal rotation speed. When the crystal rotation speed was relatively low (Fig. 4(a), natural convection occuring just beneath the interface is predominant. The solid-liquid interfacial shape of the crystal growth of ZnWO₄ became convex below 55 rpm. Forced convection stronger than natural convection was produced when the crystal rotation speed is high in Fig. 4(b). The forced convection is caused by a stream of hot liquid inside the melt going up towards the interface. The solid-liquid interfacial shape of the crystal growth of ZnWO₄ becomes concave towards the melt above 63 rpm. The fluid-flow modes help establish the freezing isotherm indicated by the line curves, allowing a convex or concave interface shape.

TABLE-3
CRYSTAL SHAPE, ROTATION SPEED AND MAXIMUM DIAMETER OF THE GROWN ZnWO₄ SINGLE CRYSTALS

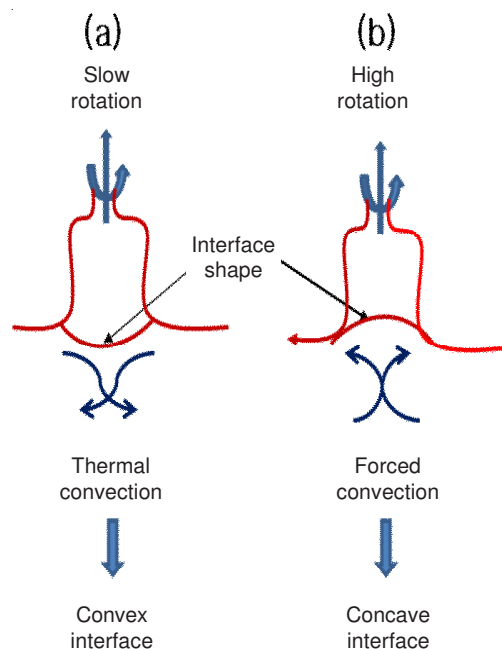| Nomination	A	B	C	D	E	F	G	H
Rotation speed (rpm)	15, 26	16	39	55	68	54, 40	46	63
Max. diamter (mm)	21	16	23	35	12	20	17	23

Fig. 4. Schematic diagram of the relationships between fluid-flowing convection models and interfacial shape at different crystal rotation speeds

The important parameters to consider in fluid-flow are the Prandtle number σ and Rayleigh number R_a, which are expressed by the following equations[8]:

$$\sigma = \eta c_p/k = \nu/k \qquad (2)$$

$$R_a = L^3\beta g(T_1\text{-}T_2)/\nu k \qquad (3)$$

where η is the viscosity, c_p is the latent heat at a constant pressure, k is the thermal diffusivity, ν is the kinetmatic viscosity, L is the dimension of the system under consideration (crucible diameter in the present case), β is the thermal expansion coefficient for the liquid, g is gravity and $(T_1\text{-}T_2) = \Delta T$ is the temperature difference in a system.

The natural convection caused by the temperature difference in a liquid is normally given by a dimensionless parameter, Grashof number G_r, which corresponds to the ratio of the viscosity to levitation due to thermal expansion of a liquid:

$$R_a = \sigma\, G_r \qquad (4)$$

On the other hand, the forced convection associated with crystal rotation is given by the dimensionless parameter, Reynolds number R_e, which is expressed as:

$$R_e = LV/\nu = d/2 \cdot \pi wd/\nu \qquad (5)$$

where d is the crystal diameter and w is the crystal rotation speed.

By normalizing the two measures of G_r and R_e with respect to the viscosity:

$$d = (4g\beta TR^3\pi^{-2})^{1/4}/w^{1/2} \qquad (6)$$

was obtained because fluid-flow interacts through drag. Eqn. 6 shows the relationship between the crystal diameter and crystal rotation speed, which makes the interface flat. It provides a linear relationship between d and $w^{-1/2}$, which means that the natural and forced convections are balanced, giving rise to a flat interface. Therefore, gas-bubble entrapment depends on fluid-flow convection modes. In this study, the pulling rate

was regulated between 0-10 mm/h. The rotation speed and diameters were regulated under consideration of fluid-flow convection of a liquid in contact with the growing interface. The gas-bubble entrapments were observed from the viewpoint of fluid-flow modes in the melt in connection with the shape of the growing solid-liquid interface. Gas-bubble entrapment can be avoided by adjusting the crystal rotation speed to make a flat or slightly concave interfacial shape to the melt. The formation of cracks in the grown crystals during the cooling process could be prevented by annealing at 800 ºC for 10 h.

Fig. 5 shows the grown single crystals of $ZnWO_4$ in the [100], [010] and [001] directions, which correspond to Table-4 (A), (B), (C) with the growth direction, rotation speed and diameter. As listed in Table-4, the rotation speed was between 40-54 rpm with a diameter of 20 mm for the [100] direction in Fig. 5(a), whereas it was 46 rpm with a diameter of 17 mm for the [101] direction in Fig. 5(b) and 63 rpm with a diameter 23 mm for the [001] direction in Fig.5(c). The formation of cracking in the grown crystals in the [001] direction during the cooling process can be prevented by annealing at 800 ºC for 10 h.

Fig. 5. The grown single crystals of $ZnWO_4$ in (a) [100], (b) [010] and (c) [001], which corresponds to Table-4 (A), (B) and (C) with the growth direction, rotation speed and diameter

TABLE-4
GROWTH CONDITIONS OF THE GROWN $ZnWO_4$ SINGLE CRYSTALS OF (A) [100], (B) [010] AND (C) [001]

Crystals conditions	A	B	C
Direction	[100]	[010]	[001]
Rotation speed (rpm)	54,40	46	63
Weight (g)	85.9	47.0	90.7
Annealing effect	No	800ºC, 10 h	800ºC, 10 h
Remark	Crack	Bubble	No crack
			No bubble

*The crystal data of A, B, C are corresponding to the crystal in Fig. 5(a), (b), (c).

Fig. 6 shows the crystal structure of the ZnWO$_4$. It is based on a distorted hexagonal close packing of O atoms with Zn and W atoms, each occupying one-fourth of the octahedral interstices. The presence of two non-equivalent oxygen atoms is responsible for the pairs of Zn-O and W-O bonds with different lengths. Therefore, both Zn and W atoms are surrounded by six oxygen atoms, forming a distorted octahedral coordination. Each chain of the ZnO$_6$ octahedra is corner-linked and the chains of WO$_6$ octahedra are edge-linked, which are also parallel to [001]. The ZnO$_6$ and WO$_6$ octahedra consist of three pairs of cation-oxygen bonds with Zn and W atoms being displaced from the center of their octahedra by *ca.* 0.29 and 0.32 Å, respectively, along the [010] direction. Since two like atoms in a unit cell are related by a center of symmetry, they are off center in the opposite sense in a manner characteristic of an antiferroelectric.
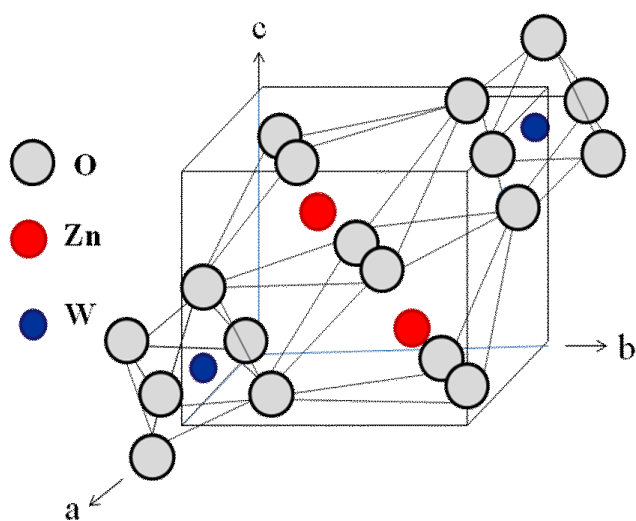

Fig. 7. Unit cell of ZnWO$_4$ projected on the (001) and (100) planes

Fig. 6. The crystal structure of the ZnWO$_4$. Each chain of the ZnO$_6$ octahedra is corner-linked, and the chains of the WO$_6$ octahedra are edge-linked, which are also parallel to [001]

Fig. 7 shows the unit cell of ZnWO$_4$ projected on the (001) and (100) planes. For the (100) planes the oxygen atoms are halfway between the reflecting planes and are located in the region of maximum field amplitude of the anomalously transmitted standing wave. Therefore, oxygen atoms absorb the transmitted wave. However, for (001) planes, oxygen atoms are displaced from the position of the maximum field amplitude, which means that they absorb less than the (100) reflection. Therefore, the intensity of the (001) reflection is *ca.* 2 to 3 times that of the (100) reflection. This difference in intensity is due to the different locations of the oxygen atoms relative to the position of the maximum field amplitude in the two reflections.

The dislocation density of ZnWO$_4$ was obtained from the etch pits on the surfaces of the grown crystals. Fig. 8 shows the etch pattern of the (010) plane of a grown ZnWO$_4$ single crystal. The dislocation density at the center of the crystal was lower than at the edge of the crystal. The features of the dislocations of the (010) plane were propagated along the [001] direction. The etch pit arrangement shows that slip occurred along the (100) plane, particularly near the edge of the crystal.
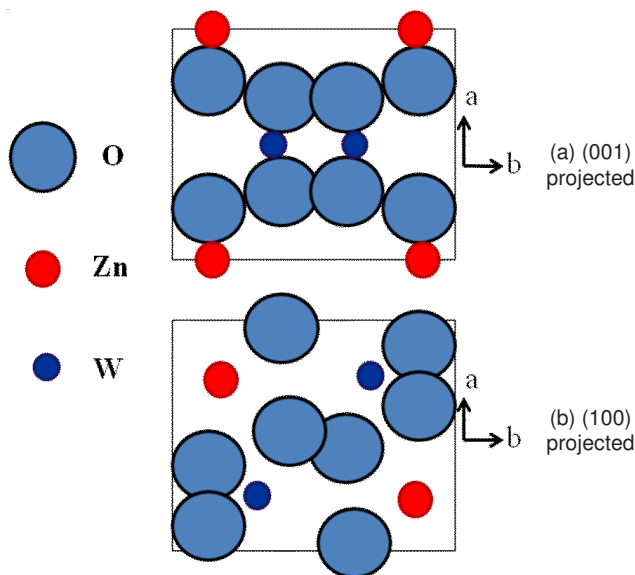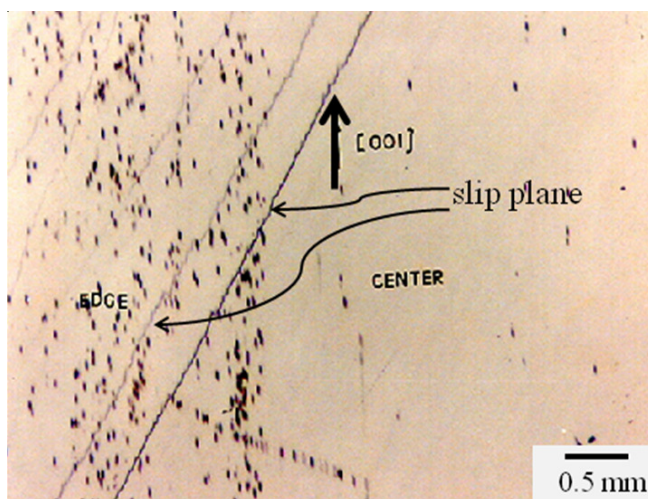

Fig. 8. Etch pattern of the (010) plane of a grown ZnWO$_4$ single crystal. The dislocation density at the center of the crystal is lower than at the edge of the crystal

It is possible that a dislocation of this type grew or slipped on either the (010) or (100) slip planes. The fact that these straight dislocations terminate abruptly near the center of the crystal would suggest that extensive cross slip had occurred in the crystal. This can happen without cross slip because the polished crystal surface is flat only on a gross scale and dislocations lying in the (010) plane can intersect this surface.

When slip in the (100) plane is concentrated in a slip band, as indicated by the presence of etch pits on the adjacent section in Fig. 8, an image appears in all anomalous transmission reflections. This probably occurs because the strain fields of the dislocations superpose and the edge components of these dislocations are slightly visible in any plane not perpendicular to them. The etch pits were similar for all crystals grown in the [001], [010], [100] directions. When a crystal is grown in the [001] direction, as is usual for maser applications, the (100) and (010) slip planes are parallel to the growth direction. Existing dislocations, either in the seed or generated in the crystal, can slip, intersect the solid-liquid interface and then

continue to propagate by growth. These arrays coincide with the low-angle grain boundaries, whose tilt could be observed under a microscope.

The crystallographic orientation of $ZnWO_4$ crystal could considered. $ZnWO_4$ has a monoclinic wolframite structure in the space group P2/c. There are two formula units per primitive cell with the lattice parameters a = 4.69263 Å, b = 5.72129 Å, c = 4.92805 Å and β = 90.6321°. Cleavage gives a (010) crystal face and etching gives rise to etch pits aligned parallel to the (100) slip plane in the [001] direction. The optic plane in $ZnWO_4$ is perpendicular to the (010) cleavage plane. The lattice parameter of b (5.72129 Å) is longer than that of a (4.69263 Å) and c (4.92805 Å). Hence, the cleavage surface propagates on the (010) plane.

The physical properties of the crystals were evaluated. The hardness of the grown crystals was similar in each direction (434, 473 and 471 kg/mm^2 in the [100], [101] and [001], respectively). The dielectric constant of the [100] direction was 68 compared to 49 and 57 in the [010] and [001] directions. The thermal expansion coefficients were 9.2, 8.8 and 7.9 × 10^{-6}/°C for the [100], [010] and [001] growth directions, respectively.

Conclusion

$ZnWO_4$ nanopowders were prepared from polymeric complex precursor using microwave irradiation. The nanopowders at 500 °C had relatively more homogeneous morphology, while the powders at 600 °C showed relatively exaggerated growth including rectangular form. The average crystalline sizes were 18-25 nm showing an ordinary tendency to increase with the temperatures from 400 to 600 °C. Single crystals of $ZnWO_4$ were grown successfully in the [100], [010] and [001] directions by the Czochralski method. The rotation speed was controlled between 40-54 rpm with a diameter of 20 mm for the [100] direction, whereas the speed was 46 rpm with a diameter of 17 mm for the [101] direction and 63 rpm with a diameter 23 mm for the [001] direction. The $ZnWO_4$ crystals had a cleavage plane of (010). The dislocation density on the (010) plane at the center of the crystal was lower than that near the edge. The etch pit arrangement shows that the (100) slip plane appeared to be most active during crystal growth. The hardness of the grown crystals was similar in each direction. The dielectric constant of the [100] direction was 68 compared to 49 in the [010] direction and 57 in the [001] direction. The thermal expansion coefficients were 9.2, 8.8 and 7.9 × 10^{-6}/°C for the [100], [010], [001] directions, respectively.

REFERENCES

1. A. Kalinko, A. Kuzmin and R.A. Evarestov, *Solid State Commun.*, **149**, 425 (2009).
2. P. Belli, R. Bernabei, F. Cappella, R. Cerulli, F.A. Danevich, B.V. Grinyov, A. Incicchitti, V.V. Kobychev, V.M. Mokina, S.S. Nagorny, L.L. Nagornaya, S. Nisi, F. Nozzoli, D.V. Poda, D. Prosperi, V.I. Tretyak and S.S. Yurchenko, *Nucl. Phys. A*, **826**, 256 (2009).
3. X. Cao, W. Wu, N. Chen, Y. Peng and Y. Liu, *Sens. Actuators B*, **137**, 83 (2009).
4. C. Yu and J.C. Yu, *Mater. Sci. Eng. B*, **141**, 16 (2009).
5. S. Lin, J. Chen, X. Weng, L. Yang and X. Chen, *Mater. Res. Bull.*, **44**, 1102 (2009).
6. M. Itoh, T. Katagiri, T. Aoki and M. Fujita, *Radiat. Measurements*, **42**, 545 (2007).
7. V. Nagirnyi, L. Jonsson, M. Kirm, A. Kotlov, A. Lushchik, I. Martinson, A. Watterich and B.I. Zadneprovski, *Radiat. Measurements*, **38**, 519 (2004).
8. S. Miyazawa, *J. Crystal Growth*, **49**, 515 (1980).
9. A. Kornylo, A. Jankowska-Frydel, B. Kuklinski, M. Grinberg, N. Kruyiak, Z. Moroz and M. Pashkowsky, *Radiat. Measurements*, **38**, 707 (2004).
10. L. Malicsko, A. Peter and W. Erfurth, *J. Crystal Growth*, **15**, 127 (1995).
11. G.B. Kumar, K. Sivaiah and S. Buddhudu, *Ceram. Int.*, **36**, 199 (2010).
12. XG. Huang and Y. Zhu, *Mater. Sci. Eng. B*, **139**, 201 (2007).
13. X. Jiang, J. Ma, J. Liu, Y. Ren, B. Lim, J. Tao and X. Zhu, *Mater. Lett.*, **61**, 4595 (2007).
14. T. Dong, Z. Li, Z. Ding, L. Wu, X. Wang and X. Fu, *Mater. Res. Bull.*, **43**, 1694 (2008).
15. A. Dodd, A. Mckinley, T. Tsuzuki and M. Saunders, *J. Eur. Ceram. Soc.*, **29**, 139 (2009).
16. X. Zhao, W. Yao, Y. Wu, S. Zhang. H. Yang and Y. Zhu, *J. Solid State Chem.*, **179**, 2562 (2006).
17. F.-S. Wen, X. Zhao, H. Huo, J.-S. Chen, E. Shu-Lin and J.-H. Zhang, *Mater. Lett.*, **5**, 152 (2002).
18. G. Huang, C. Zhang and Y. Zhu, *J. Alloys Comp.*, **432**, 269 (2007).
19. H. Fu, J. Lin, L. Zhang and Y. Zhu, *Appl. Catal. A: Gen.*, **306**, 58 (2006).
20. K. Kuribayashi, M. Yoshimura, T. Ohta and T. Sata, *Bull. Chem. Soc. (Japan)*, **50**, 2932 (1977).
21. N.G. Eror and H.U. Anderson, *Mater. Res. Soc. Symp. Proc.*, **73**, 571 (1986).
22. M. Kakihana, *J. Sol-Gel Sci. Tech.*, **6**, 7 (1996).
23. M.P. Pechini, U.S. Pat., 3330697 (1967).
24. S. Kumar, G.L. Messing and W.B. White, *J. Am. Ceram. Soc.*, **76**, 617 (1993).
25. M. Yoshimura, J. Ma and M. Kakihana, *J. Am. Ceram. Soc.*, **81**, 2721 (1998).
26. P.A. Lessing, *Am. Ceram. Soc. Bull.*, **68**, 1002 (1989).
27. M. Kakihara, M. Yoshimura, H. Mazaki, H. Yasuoka and L. Borjesson, *J. Appl. Phys.*, **71**, 3904 (1992).
28. C. Jansen, A. Arafat, A.K. Barakat, H.Van Bekkum, in eds.: M.L. Occelli and H. Robson, Synthesis of Microporous Materials, Van Nostrand Reinhold, New York, Vol. 1, p. 507 (1992).
29. I. Girnus, K. Hoffmann, F. Marlow and J. Caro, *Micropor. Mater.*, **2**, 537 (1994).
30. X.C. Xu, W.S. Yang, J. Liu and L.W. Lin, *Adv. Mater.*, **3**, 195 (2000).
31. K.J. Rao, B. Vaidhyanathan, M. Gaguli and P.A. Ramakrishnan, *Chem. Mater.*, **11**, 882 (1999).
32. J. Bi, L. Wu, Z. Li, Z. Ding, X. Wang and X. Fu, *J. Alloys Comp.*, **480**, 684 (2009).
33. K.N.P. Kumar, K. Keizer and A.J. Bureggraaf, *J. Mater. Chem.*, **3**, 1141 (1993).